Highly Antiproliferative Ruthenium(II) and Osmium(II) Arene Complexes with Paullone-Derived Ligands

Wolfgang F. Schmid, Roland O. John, Vladimir B. Arion,* Michael A. Jakupec, and Bernhard K. Keppler*

Institute of Inorganic Chemistry, University of Vienna, Währingerstrasse 42, A-1090 Vienna, Austria

Received August 9, 2007

The paullones are known as inhibitors of cyclin-dependent kinases and glycogen synthase kinase-3. However, their low aqueous solubility and bioavailability impeded their medicinal application. To overcome these problems, we developed paullone-based organic ligands and prepared organometallic complexes of the general formula [$M^{II}Cl(\eta^6$-*p*-cymene)HL]Cl (**1**, HL = $\mathbf{HL^1}$; **2**, HL = $\mathbf{HL^2}$; **a**, M = Ru; **b**, M = Os). The compounds have been characterized by electrospray ionization mass spectrometry, IR, UV–vis, NMR spectroscopy, X-ray diffraction, conductivity measurements, and cyclic voltammetry. In addition, their antiproliferative activity in three human cancer cell lines has been assayed. The IC_{50} values (in the submicromolar to very low micromolar concentration range) indicate their high antiproliferative activity in all three cell lines, making them potential candidates for further development as antitumor drugs. The hydrolysis behavior and reactivity of **1** and **2** toward 5′-GMP are also reported.

Introduction

Since their discovery as potent inhibitors of cyclin-dependent kinases (CDKs),[1–3] the paullones (Chart 1) have been shown to inhibit also other relevant intracellular proteins, *e.g.*, glycogen synthase kinase-3 and mitochondrial malate dehydrogenase.[4] Compounds with a modified lactam unit have been found to inhibit sirtuins, which are likely involved in the pathogenesis of viral diseases and cancer. Their inhibitory potency is higher than that of the unsubstituted parent paullones.[5]

Kunick et al. reported a large number of paullone derivatives that are capable of inhibiting tumor cell growth *in vitro* and established structure–activity relationships.[6,7] Intriguingly, a 12-Boc-substituted paullone (B) and a lactam-modified kenpaullone methylthioimidate (C; Chart 1) display remarkable antiproliferative activity, although their CDK-inhibitory potency is reduced.[1]

In an effort to investigate the effect of metalation on the biological properties of lactam-modified paullones, we have previously prepared the gallium(III) complex $[Ga^{III}(\mathbf{L^1})_2]Cl$ with a paullone-based ligand shown in Scheme 1.[8] This complex was found to inhibit cancer cell proliferation in low micromolar concentrations but exhibited neither sufficient aqueous solubility nor hydrolytic stability for any further application. The design of novel bidentate paullone ligands and investigation of their binding ability to the kinetically more inert ruthenium(II) resulted in stable complexes of the composition $[Ru^{II}Cl(DMSO)L_2]Cl$ (DMSO = dimethyl sulfoxide), which also showed remarkable antiproliferative activity but limited aqueous solubility.[9]

Chart 1. Structures of Kenpaullone (A), Its 12-Boc Derivative (B), and Its Methylthioimidate (C)

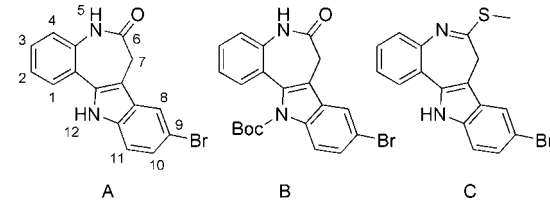

Binding of organic ligands to organometallic moieties may serve as another means to increasing solubility and bioavailability[10] and preserving or even enhancing their antitumor activity.[11–14] The insufficient bioavailability and solubility of

* To whom correspondence should be addressed. E-mail: vladimir.arion@univie.ac.at (V.B.A.), bernhard.keppler@univie.ac.at (B.K.K.). Fax: +43 1 4277 52630 (V.B.A.), +43 1 4277 52680 (B.K.K.).

(1) Zaharewitz, D. W.; Gussio, R.; Leost, M.; Senderowitz, A. M.; Lahusen, T.; Kunick, C.; Meijer, L.; Sausville, E. A. *Cancer Res.* **1999**, *59*, 2566–2569.

(2) Huwe, A.; Mazitschek, R.; Giannis, A. *Angew. Chem., Int. Ed.* **2003**, *19*, 2122–2138.

(3) Kunick, C. *Arch. Pharm. (Weinheim, Ger.)* **1992**, *325*, 297–299.

(4) Knockaert, M.; Wieking, K.; Schmitt, S.; Leost, M.; Grant, K. M.; Mottram, J. C.; Kunick, C.; Meijer, L. *J. Biol. Chem.* **2002**, *277*, 25493–25501.

(5) Trapp, J.; Jochum, A.; Meier, R.; Saunders, L.; Marshall, B.; Kunick, C.; Verdin, E.; Goekjian, P.; Sippl, W.; Jung, M. *J. Med. Chem.* **2006**, *49*, 7307–7316.

(6) Kunick, C.; Schultz, C.; Lemcke, T.; Zaharevitz, D. W.; Gussio, R.; Jalluri, R. K.; Sausville, E. A.; Leost, M.; Meijer, L. *Bioorg. Med. Chem. Lett.* **2000**, *10*, 567–569.

(7) Pies, T.; Schaper, K.-J.; Leost, M.; Zaharevitz, D. W.; Gussio, R.; Meijer, L.; Kunick, C. *Arch. Pharm. Pharm. Med. Chem.* **2004**, *337*, 486–492.

(8) Dobrov, A.; Arion, V. B.; Kandler, N.; Ginzinger, W.; Jakupec, M. A.; Rufiñska, A.; Graf von Keyserlingk, N.; Galanski, M.; Kowol, C.; Keppler, B. K. *Inorg. Chem.* **2006**, *45*, 1945–1950.

(9) Schmid, W. F.; Zorbas-Seifried, S.; John, R. O.; Arion, V. B.; Jakupec, M. A.; Roller, A.; Galanski, M.; Chiorescu, I.; Zorbas, H.; Keppler, B. K. *Inorg. Chem.* **2007**, *46*, 3645–3656.

(10) Barton, M.; Atwood, J. D. *J. Coord. Chem.* **1991**, *24*, 43–67.

(11) Vock, C. A.; Scolaro, C.; Phillips, A. D.; Scopelliti, R.; Sava, G.; Dyson, P. J. *J. Med. Chem.* **2006**, *49*, 5552–5561.

(12) Attila-Gokcumen, G. E.; Williams, D. S.; Bregman, H.; Pagano, N.; Meggers, E. *Chem. Biol. Chem.* **2006**, *7*, 1443–1450.

(13) Morris, R. E.; Aird, R. E.; Murdoch, P. del S.; Chen, H.; Cummings, J.; Hughes, N. D.; Parsons, S.; Parkin, A.; Boyd, G.; Jodrell, D. I.; Sadler, P. J *J. Med. Chem.* **2001**, *44*, 3616–3621.

(14) Yan, Y. K.; Melchart, M.; Habtemariam, A.; Sadler, P. J. *Chem. Commun.* **2005**, 4764–4776.

10.1021/om700813c CCC: $37.00
Publication on Web 11/20/2007

Scheme 1. Synthesis of Ligands and Complexes[a]

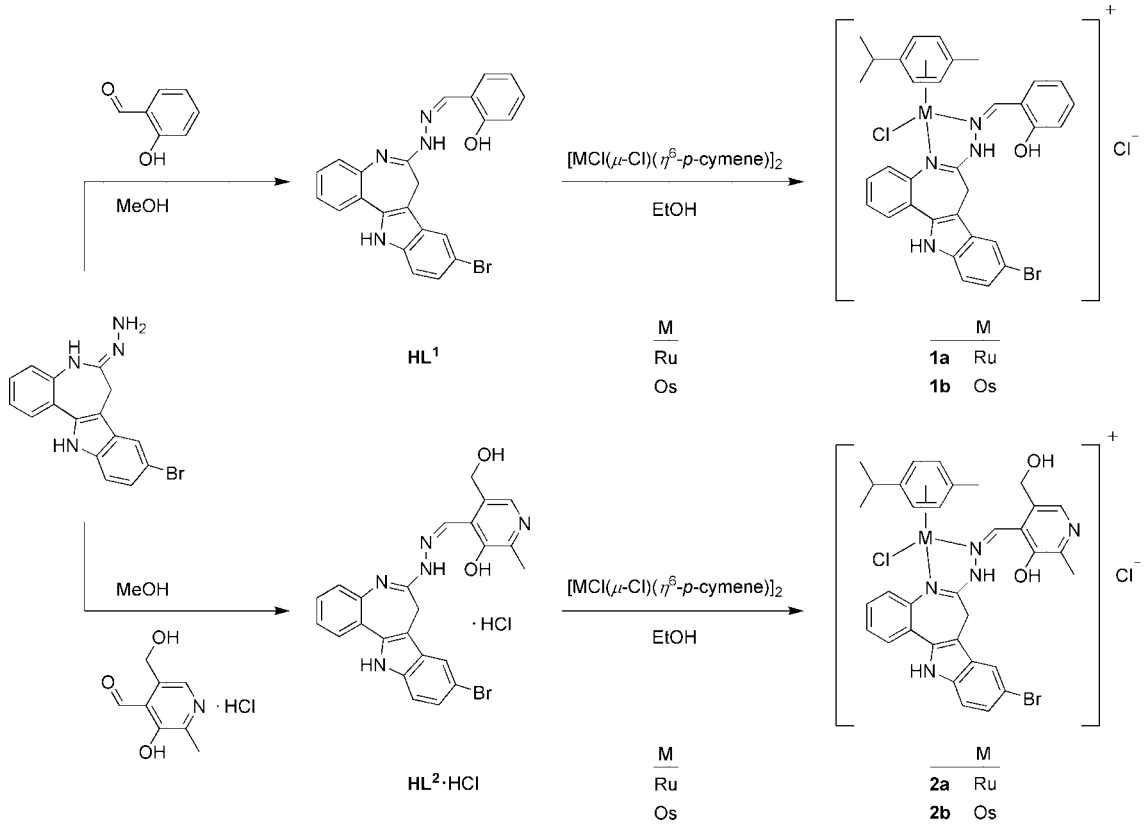

[a] In the X-ray structures of $\mathbf{HL^1}\cdot HNO_3$, **1a**, and **1b**, the Schiff base resulted from the condensation reaction of the paullone hydrazone and the aldehyde is found in the *E* configuration relative to the formed azomethine bond, whereas it is *Z*-configured in **2b** (*vide infra*). The ligands are drawn in the *Z* configuration for all compounds in this scheme.

the parent paullones, which impeded their systemic application, prompted us to prepare the paullone ligands $\mathbf{HL^1}$ and $\mathbf{HL^2}$ shown in Scheme 1 and to investigate their reactions with $[M^{II}Cl(\mu\text{-}Cl)(\eta^6\text{-}p\text{-cymene})]_2$, where M = Ru, Os.

We show in this paper that these reactions give rise to complexes of the general formula $[M^{II}Cl(\eta^6\text{-}p\text{-cymene})HL]Cl$ (**1**, HL = $\mathbf{HL^1}$; **2**, HL = $\mathbf{HL^2}$; **a**, M = Ru; **b**, M = Os), which exhibit increased aqueous solubility compared to the metal-free paullone ligands and higher solvolysis stability than $[Ga^{III}(\mathbf{L^1})_2]Cl$.[8] This allowed assaying their antiproliferative properties *in vitro* in three cancer cell lines. We report on the first organometallic ruthenium(II) and osmium(II) compounds with potentially tridentate paullone-based ligands bound to the metal in a bidentate fashion and demonstrate their remarkably high antiproliferative activity. The structural and spectroscopic characterization of the paullone ligands and the paullone-based organometallic compounds, both in the solid state and in solution, is described. Because various tumor-inhibiting ruthenium complexes are known to form DNA adducts, the interactions with 5′-GMP as a DNA model nucleotide have also been studied.

Experimental Section

Starting Materials. *N*-(9-Bromo-7,12-dihydroindolo[3,2-*d*][1]-benzazepin-6(5*H*)-yliden-*N*′-(2-hydroxybenzylidene)azine ($\mathbf{HL^1}$),[8] $[Ru^{II}Cl(\mu\text{-}Cl)(\eta^6\text{-}p\text{-cymene})]_2$,[15] and $[Os^{II}Cl(\mu\text{-}Cl)(\eta^6\text{-}p\text{-cymene})]_2$[16] have been prepared according to published protocols. Tetrahydrofuran (THF) and ethanol were dried using standard procedures. 2-Hydroxybenzaldehyde and 3-hydroxy-5-(hydroxymethyl)-2-methylpyridinium-4-carbaldehyde chloride (vitamin B6) were purchased from Fluka and used without further purification.

Synthesis of Ligands and Metal Complexes. *N*-(9-Bromo-7, 12-dihydroindolo[3,2-*d*][1]benzazepin-6-yl)-*N*′-[3-hydroxy-5-(hydroxymethyl)-2-methylpyridin-4-yl-methylene]azinium Chloride ($\mathbf{HL^2}\cdot$HCl). A mixture of 9-bromo-7,12-dihydroindolo[3,2-*d*][1]benzazepin-6-ylhydrazine (1.02 g, 3 mmol) and 3-hydroxy-5-(hydroxymethyl)-2-methylpyridin-4-carbaldehyde (pyridoxal) hydrochloride (0.67 g, 3.3 mmol) was refluxed in methanol (45 mL) for 45 min, allowed to cool to room temperature, and left to stand at 4 °C for 2 h. The bright-orange precipitate was filtered off, washed with methanol, and dried in vacuo. Yield: 1.36 g, 86%. Anal. Calcd for $C_{24}H_{21}BrClN_5O_2\cdot 0.2MeOH$: C, 54.51; H, 4.12; Br, 14.99; Cl, 6.65; N, 13.13. Found: C, 54.59; H, 4.02; Br, 14.70; Cl, 6.50; N, 13.16. ESI-MS: positive, *m*/*z* 514 $[\mathbf{HL^2} + Na]^+$, 492 $[\mathbf{HL^2} + H]^+$; negative, *m*/*z* 526 $[\mathbf{HL^2} + Cl]^-$, 490 $[\mathbf{HL^2} - H]^-$. IR spectrum (selected bands, KBr, ν_{max}, cm^{-1}): 3301 (NH), 3195 (NH), 2723, 2679, 1956, 1611 (CN), 1538, 1399, 754, 747 (CH_{arom}). UV–vis spectrum [methanol, λ_{max}, nm (ϵ, M^{-1} cm^{-1})]: 229 (44 370), 318 (29 940), 380 (11 510), 420sh (10600). ^{1}H NMR [400.13 MHz, DMSO-d_6, δ_H, ppm, exocyclic amidine double-bond nonprimed, endocyclic primed, ratio exo:endo = 0.59:0.41]: 2.54 (s, 3H, H^{21}), 2.74 (s, 3H′, $H^{21'}$), 3.84 (s, 2H, H^7), 4.00 (s, 2H′, $H^{7'}$), 4.77 (s, 2H, H^{16}), 4.81 (s, 2H′, $H^{16'}$), 5.65 (br s, H^{17} and $H^{17'}$), 7.29 (d, ^3J = 8.4 Hz, 1H′, $H^{10'}$), 7.32 (d, ^3J = 8.6 Hz, 1H, H^{10}), 7.35 (t, ^3J = 7.4 Hz, 1H′), 7.44 (m, 2H and 3H′), 7.51 (t, ^3J

(15) Bennett, M. A.; Smith, A. K. *J. Chem. Soc., Dalton Trans.* **1974**, 233–241.

(16) Kiel, W. A.; Ball, G.; Graham, A. G. *J. Organomet. Chem.* **1990**, *383*, 481–496.

(17) Barette, W. C., Jr.; Johnson, H. W., Jr.; Sawyer, D. T *Anal. Chem.* **1984**, *56*, 1890–1898.

= 7.5 Hz, 1H), 7.64 (d, ^3J = 7.8 Hz, 1H), 7.80 (d, ^3J = 7.3 Hz, 1H′), 7.84 (d, ^3J = 7.6 Hz, 1H), 7.88 (s, 1H′, H$^{8'}$), 7.95 (s, 1H, H^8), 8.15 (s, 1H, H^{18}), 8.20 (s, 1H′, H$^{18'}$), 8.76 (s, 1H′, H$^{15'}$), 8.90 (s, 1H, H^{15}), 10.70 (br s, 1H, H^5), 12.01 (s, 1H′, H$^{12'}$), 12.07 (s, 1H, H^{12}), 14.05 (br s, 1H, H$^{13'}$), H^{20} and H$^{20'}$ not detected. ^{13}C NMR [100.63 MHz, DMSO-d_6, δ_C, ppm, exocyclic amidine double-bond nonprimed, endocyclic primed]: 15.91 (C^{21} and C$^{21'}$), 21.80 (C^7), 22.77 (C$^{7'}$), 58.89 (C$^{16'}$), 59.21 (C^{16}), 90.06, 107.97 (C$_q$), 110.76 (C$_q$), 112.81 (C$_q$), 112.85 (C$_q$), 114.58, 114.63, 121.07, 121.47, 123.32 (C$_q$), 123.91 (C$_q$), 124.36, 125.06, 125.49, 125.80, 128.16, 128.30, 128.53 (C$_q$), 128.68 (C$_q$), 129.28, 129.54, 134.86 (C$_q$), 135.90 (C$_q$), 136.77 (C$_q$), 136.83 (C$_q$), 137.08 (2 C$_q$). Mp: 240 °C (dec).

Ruthenium(II) and Osmium(II) Arene Complexes of HL^1, General Procedure A. A mixture of *N*-(9-bromo-7,12-dihydroindolo[3,2-*d*][1]benzazepin-6(5*H*)-yliden-*N*′-(2-hydroxybenzylidene)azine (0.44 g, 1.0 mmol) and [M^{II}Cl(μ-Cl)(η^6-*p*-cymene)]$_2$ (M = Ru, Os; Ru, 0.31 g; Os, 0.39 g, 0.5 mmol) was stirred in ethanol (45 mL) for 1 h at room temperature. The yellow precipitate was filtered off, washed with ethanol, and dried in vacuo.

Ruthenium(II) and Osmium(II) Arene Complexes of HL^2, General Procedure B. *N*-(9-Bromo-7,12-dihydroindolo[3,2-*d*][1]benzazepin-6-yl)-*N*′-(3-hydroxy-5-(hydroxymethyl)-2-methylpyridin-4-ylmethylene)azinium chloride (0.53 g, 1.0 mmol) and [M^{II}Cl(μ-Cl)(η^6-*p*-cymene)]$_2$ (M = Ru, Os; Ru, 0.31 g; Os, 0.39 g, 0.5 mmol) were stirred in ethanol (50 mL) at 40 °C for 24 h and allowed to cool to room temperature. The mixture was filtered and left to stand at 4 °C for 2 weeks. (Os: After 1 week, 25 mL of hexane was added.) The crystals (Ru, red; Os, brown) were filtered off, washed with diethyl ether, and dried in vacuo.

(η^6-*p*-Cymene)[*N*-(9-bromo-7,12-dihydroindolo[3,2-*d*][1]benzazepin-κ*N*-6-yl)-*N*′-κ*N*-(2-hydroxybenzylidene)azine]chlororuthenium(II) Chloride, [RuCl(cymene)HL^1]Cl (1a). General procedure A. Yield: 0.64 g, 81%. Anal. Calcd for $C_{33}H_{31}BrCl_2N_4ORu \cdot EtOH \cdot 0.3H_2O$: C, 52.35; H, 4.72; Br, 9.95; Cl, 8.83; N, 6.98. Found: C, 52.21; H, 4.63; Br, 9.90; Cl, 8.81; N, 7.17. ESI-MS: positive, *m*/*z* 703 [RuCl(cymene)**HL^1** − HCl − H + Na]$^+$, 681 [RuCl(cymene)**HL^1** − HCl]$^+$; negative, *m*/*z* 715 [RuCl(cymene)**HL^1** − 2H]$^-$, 679 [RuCl(cymene)**HL^1** − HCl − 2H]$^-$. IR spectrum (selected bands, KBr, ν_{max}, cm^{-1}): 3360 (NH), 3183 (NH), 2971 (CH), 2760, 1610 (CN), 1590, 1570, 1454, 771, 755 (CH$_{arom}$). UV–vis spectrum [methanol, λ_{max}, nm (ϵ, M^{-1} cm^{-1})]: 209 (49 140), 316 (24 520), 235sh (37 300), 360sh (10 300). ^{1}H NMR (400.13 MHz, DMSO-d_6, δ_H, ppm): 0.34 (d, ^3J = 6.8 Hz, 3H, H^{28} or H^{29}), 0.44 (d, ^3J = 6.8 Hz, 3H, H^{28} or H^{29}), 1.75 (sept, ^3J = 6.8 Hz, 1H, H^{27}), 2.13 (s, 3H, H^{26}), 3.08 (d, ^3J = 14.6 Hz, 1H, H$^7{}_a$), 4.21 (d, ^3J = 6.0 Hz, 1H, H^{25}), 4.31 (d, ^3J = 6.2 Hz, 1H, H^{23}), 4.48 (d, ^3J = 14.5 Hz, 1H, H$^7{}_b$), 4.78 (m, 2H, H^{22} and H^{24}), 7.06 (d, ^3J = 8.2 Hz, 1H, H^{19}), 7.06 (t, ^3J = 7.4 Hz, 1H, H^{17}), 7.34 (d, ^3J = 8.6 Hz, 1H, H^{10}), 7.48 (t, ^3J = 7.8 Hz, 1H, H^{18}), 7.51 (d, ^3J = 8.8 Hz, 1H, H^{11}), 7.54 (m, 1H, H^2), 7.55 (m, 1H, H^3), 7.86 (m, 1H, H^1), 7.91 (s, 1H, H^8), 8.30 (d, ^3J = 8.0 Hz, 1H, H^4), 8.36 (d, ^3J = 7.7 Hz, 1H, H^{16}), 8.89 (s, 1H, H^{15}), 10.79 (s, 1H, H^{20}), 12.26 (s, 1H, H^{12}), 14.72 (br s, 1H, H^{13}). ^{13}C NMR (100.63 MHz, DMSO-d_6, δ_C, ppm): 19.20 (C^{26}), 21.14 (C^{29}), 22.16 (C^{28}), 23.04 (C^7), 30.91 (C^{27}), 82.61 (C^{22}), 84.19 (C^{25}), 84.66 (C^{24}), 89.83 (C^{23}), 101.37 (C^{23a}), 106.47 (C^{25a}), 109.35 (C^{7a}), 112.80 (C^9), 114.56 (C^{11}), 116.57 (C^{19}), 119.78 (C^{17}), 120.90 (C^{15a}), 121.50 (C^8), 125.01 (C^{12b}), 125.82 (C^{10}), 126.91 (C^2), 127.56 (C^1), 128.07 (C^{7b}), 128.91 (C^3), 129.69 (C^4), 132.15 (C^{16}), 134.64 (C^{18}), 135.03 (C^{12a}), 137.26 (C^{11a}), 147.30 (C^{4a}), 157.85 (C^{15}), 157.99 (C^6), 158.59 (C^{19a}). Mp: 180 °C (dec). X-ray diffraction quality single crystals of **1a**·C_2H_5OH were grown by slow diffusion of diethyl ether into an ethanolic solution of **1a**.

(η^6-*p*-Cymene)[*N*-(9-bromo-7,12-dihydroindolo[3,2-*d*][1]benzazepin-κ*N*-6-yl)-*N*′-κ*N*-(2-hydroxybenzylidene)azine]chloroosmium(II) Chloride, [OsCl(cymene)HL^1]Cl (1b). General procedure A. Yield: 0.71 g, 77%. Anal. Calcd for $C_{33}H_{31}BrCl_2N_4OOs \cdot 1.25EtOH \cdot H_2O$: C, 46.53; H, 4.46; N, 6.11. Found: C, 46.57; H, 4.12; N, 5.90. ESI-MS: positive, *m*/*z* 805 [OsCl(cymene)**HL^1**]$^+$, 791 [OsCl(cymene)**HL^1** − HCl − H + Na]$^+$, 769 [OsCl(cymene)**HL^1** − HCl]$^+$; negative, *m*/*z* 884 [OsCl(cymene)**HL^1** − H + Cl + EtOH]$^-$, 803 [OsCl(cymene)**HL^1** − 2H]$^-$, 767 [OsCl(cymene)**HL^1** − HCl − 2H]$^-$. IR spectrum (selected bands, KBr, ν_{max}, cm^{-1}): 3360 (NH), 3200 (NH), 2970 (CH), 2751, 1609 (CN), 1588, 1570, 1454, 771, 754 (CH$_{arom}$). UV–vis spectrum [methanol, λ_{max}, nm (ϵ, M^{-1} cm^{-1})]: 315 (33 030), 220sh (60 100), 380sh (11 800), 440sh (5700). ^{1}H NMR (400.13 MHz, DMSO-d_6, δ_H, ppm): 0.32 (d, ^3J = 6.8 Hz, 3H, H^{29}), 0.39 (d, ^3J = 6.8 Hz, 3H, H^{28}), 1.67 (sept, ^3J = 6.8 Hz, 1H, H^{27}), 2.19 (s, 3H, H^{26}), 3.26 (d, ^3J = 14.6 Hz, 1H, H$^7{}_a$), 4.43 (d, ^3J = 5.5 Hz, 1H, H^{25}), 4.56 (d, ^3J = 5.7 Hz, 1H, H^{23}), 4.59 (d, ^3J = 14.8 Hz, 1H, H$^7{}_b$), 4.95 (d, ^3J = 5.6 Hz, 1H, H^{22}), 5.08 (d, ^3J = 5.5 Hz, 1H, H^{24}), 7.02 (t, ^3J = 7.6 Hz, 1H, H^{17}), 7.04 (d, ^3J = 8.3 Hz, 1H, H^{19}), 7.33 (d, ^3J = 8.6 Hz, 1H, H^{10}), 7.45 (t, ^3J = 7.8 Hz, 1H, H^{18}), 7.49 (d, ^3J = 8.8 Hz, 1H, H^{11}), 7.51 (m, 1H, H^2), 7.52 (m, 1H, H^3), 7.83 (d, ^3J = 5.9 Hz, 1H, H^1), 7.92 (s, 1H, H^8), 8.15 (d, ^3J = 7.9 Hz, 1H, H^{16}), 8.16 (m, 1H, H^4), 8.75 (s, 1H, H^{15}), 10.76 (s, 1H, H^{20}), 12.21 (s, 1H, H^{12}), 15.23 (br s, 1H, H^{13}). ^{13}C NMR (100.63 MHz, DMSO-d_6, δ_C, ppm): 18.95 (C^{26}), 21.73 (C^{29}), 22.24 (C^7), 22.28 (C^{28}), 31.28 (C^{27}), 72.96 (C^{22}), 74.72 (C^{25}), 76.49 (C^{24}), 81.22 (C^{23}), 92.62 (C^{23a}), 100.46 (C^{25a}), 109.42 (C^{7a}), 112.83 (C^9), 114.59 (C^{11}), 116.47 (C^{19}), 119.85 (C^{17}), 120.72 (C^{15a}), 121.52 (C^8), 124.88 (C^{12b}), 125.87 (C^{10}), 127.19 (C^2), 127.49 (C^1), 128.02 (C^{7b}), 128.92 (C^3), 130.02 (C^4), 132.59 (C^{16}), 134.49 (C^{18}), 134.91 (C^{12a}), 137.22 (C^{11a}), 146.92 (C^{4a}), 157.61 (C^{15}), 158.62 (C^{19a}), 159.18 (C^6). Mp: 180 °C (dec). Single crystals of **1b**·C_2H_5OH suitable for X-ray diffraction study were obtained by slow diffusion of diethyl ether into a solution of **1b** in ethanol.

(η^6-*p*-Cymene)[*N*-(9-bromo-7,12-dihydroindolo[3,2-*d*][1]benzazepin-κ*N*-6-yl)-*N*′-κ*N*-(3-hydroxy-5-(hydroxymethyl)-2-methylpyridin-4-yl-methylene)azine]chlororuthenium(II) Chloride, [RuCl(cymene)HL^2]Cl (2a). General procedure B. Yield: 0.34 g, 41%. Anal. Calcd for $C_{34}H_{34}BrCl_2N_5ORu \cdot 2.5H_2O$: C, 48.52; H, 4.67; Br, 9.49; Cl, 8.43; N, 8.32. Found: C, 48.59; H, 4.82; Br, 9.47; Cl, 8.38; N, 8.15. ESI-MS: positive, *m*/*z* 784 [RuCl(cymene)**HL^2** − H + Na]$^+$, 762 [RuCl(cymene)**HL^2**]$^+$, 726 [RuCl(cymene)**HL^2** − HCl]$^+$; negative, *m*/*z* 796 [RuCl(cymene)**HL^2** − H + Cl]$^-$, 760 [RuCl(cymene)**HL^2** − 2H]$^-$. IR spectrum (selected bands, KBr, ν_{max}, cm^{-1}): 3402 (NH), 3280 (NH), 3065 (CH$_{arom}$), 2966 (CH), 1565, 1540, 1517, 1493, 1388, 1307, 1063, 1037, 771 (CH$_{arom}$). UV–vis spectrum [methanol, λ_{max}, nm (ϵ, M^{-1} cm^{-1})]: 209 (55 830), 318 (28 120), 395 (7610), 500sh (3600). ^{1}H NMR (400.13 MHz, DMSO-d_6, δ_H, ppm): 0.46 (d, ^3J = 6.7 Hz, 3H, H^{29}), 0.63 (d, ^3J = 6.8 Hz, 3H, H^{28}), 1.99 (sept, ^3J = 6.7 Hz, 1H, H^{27}), 2.09 (s, 3H, H^{26}), 2.69 (s, 3H, H^{21}), 2.98 (d, ^3J = 14.6 Hz, 1H, H$^7{}_a$), 4.06 (d, ^3J = 14.5 Hz, 1H, H$^7{}_b$), 4.66 (d, ^3J = 14.2 Hz, 1H, H^{16}), 4.69 (d, ^3J = 5.8 Hz, 1H, H^{23}), 4.99 (d, ^3J = 14.1 Hz, 1H, H^{16}), 5.07 (d, ^3J = 5.9 Hz, 1H, H^{22}), 5.36 (d, ^3J = 5.8 Hz, 1H, H^{25}), 5.66 (d, ^3J = 5.9 Hz, 1H, H^{24}), 5.79 (br s, 1H, H^{17}), 7.29 (d, ^3J = 8.6 Hz, 1H, H^{10}), 7.44 (m, 1H, H^2), 7.47 (d, ^3J = 8.8 Hz, 1H, H^{11}), 7.47 (m, 1H, H^3), 7.79 (s, 1H, H^8), 7.80 (m, 1H, H^1), 8.05 (s, 1H, H^{19}), 8.26 (d, ^3J = 7.0 Hz, 1H, H^4), 8.42 (s, 1H, H^{15}), 12.16 (s, 1H, H^{12}), 14.43 (br s, 1H, H^{13}), H^{20} not detected. ^{13}C NMR (100.63 MHz, DMSO-d_6, δ_C, ppm): 16.22 (C^{21}), 19.20 (C^{26}), 21.45 (C^{29}), 22.48 (C^{28}), 24.53 (C^7), 30.95 (C^{27}), 59.21 (C^{16}), 84.21 (C^{22}), 84.77 (C^{25}), 85.14 (C^{24}), 89.12 (C^{23}), 101.90 (C^{23a}), 104.81 (C^{25a}), 110.18 (C^{7a}), 112.62 (C^9), 114.47 (C^{11}), 120.90 (C^8), 125.04 (C^{12b}), 125.42 (C^{10}), 125.92 (C^2), 127.13 (C^{19}), 127.24 (C^1), 128.26 (C^{7b}), 128.45 (C^3), 130.11 (C^4), 130.81 (C^{15b}), 135.37 (C^{12a}), 137.10 (C^{11a}), 138.91 (C^{15a}), 145.71 (C^{15}), 146.57 (C^{19a}), 148.38 (C^{4a}), 154.77 (C^{19b}), 165.63 (C^6). Mp: 200 °C (dec).

Table 1. Selected Bond Lengths (Å) and Angles (deg) for $HL^1 \cdot HNO_3$, 1a, 1b, and 2b

	$HL^1 \cdot HNO_3$	1a	1b	2b[a]
M−arene centroid		1.683	1.680	1.675
M−N2		2.092(3)	2.112(9)	2.102(4)
M−N4		2.090(4)	2.087(9)	2.062(4)
M−Cl1		2.3862(11)	2.391(2)	2.4022(13)
N2−C12	1.3161(19)	1.291(5)	1.320(13)	1.321(6)
C12−N3	1.322(2)	1.353(5)	1.333(12)	1.326(6)
N4−C13	1.290(2)	1.291(6)	1.301(15)	1.302(6)
N2−M−N4		76.94(13)	76.8(3)	75.80(15)
N2−M−Cl1		85.99(11)	85.1(3)	86.20(11)
N4−M−Cl1		85.44(11)	84.3(3)	84.93(11)
$\Theta_{N2-C12-N3-N4}$	−10.2(2)	−3.6(6)	−3.0(14)	0.0(6)
$\Theta_{N3-N4-C13-C14}$	175.99(14)	177.9(4)	176.7(12)	1.8(7)
$\Theta_{N4-C13-C14-C19}$	−4.1(2)	115.0(5)	111.7(15)	37.6(8),−39.3(8)[b]
$\Theta_{N1-C5-C6-C7}$	27.0(2)	−35.4(7)	−35.9(17)	36.1(7)

[a] Values are given for the first independent molecule. [b] Values for the corresponding angles $\Theta_{N4-C13-C14-C18}$ and $\Theta_{N9-C47-C48-C52}$ in the first and second independent molecule, respectively.

(η^6-*p*-Cymene)[*N*-(9-bromo-7,12-dihydroindolo[3,2-*d*][1]benzazepin-κ*N*-6-yl)-*N*′-κ*N*-(3-hydroxy-5-(hydroxymethyl)-2-methylpyridin-4-yl-methylene)azine]chloroosmium(II) Chloride, [OsCl(cymene)HL^2]Cl (2b). General procedure B. Yield: 0.61 g, 65%. Anal. Calcd for $C_{34}H_{34}BrCl_2N_5OOs \cdot 0.8EtOH \cdot 2H_2O$: C, 44.61; H, 4.50; N, 7.31. Found: C, 44.57; H, 4.29; N, 7.28. ESI-MS: positive, *m*/*z* 872 [OsCl(cymene)$\mathbf{HL^2}$ − H + Na]$^+$, 850 [OsCl(cymene)$\mathbf{HL^2}$]$^+$, 814 [OsCl(cymene)$\mathbf{HL^2}$ − HCl]$^+$; negative, *m*/*z* 884 [OsCl(cymene)$\mathbf{HL^2}$ − H + Cl]$^-$, 848 [OsCl(cymene)$\mathbf{HL^2}$ − HCl − 2H]$^-$. IR spectrum (selected bands, KBr, ν_{max}, cm^{-1}): 3367 (NH), 3264 (NH), 2966 (CH), 1558, 1540, 1494, 1388, 1307, 1063, 1041, 775 (CH_{arom}). UV–vis spectrum [methanol, λ_{max}, nm (ϵ, M^{-1} cm^{-1})]: 210 (55 030), 316 (32 210), 399 (9860), 430 (10 240), 520sh (5400). ^{1}H NMR (400.13 MHz, DMSO-d_6, δ_H, ppm): 0.40 (d, ^3J = 6.7 Hz, 3H, H^{29}), 0.56 (d, ^3J = 6.8 Hz, 3H, H^{28}), 1.86 (sept, ^3J = 6.8 Hz, 1H, H^{27}), 2.20 (s, 3H, H^{26}), 2.70 (s, 3H, H^{21}), 3.18 (d, ^3J = 14.5 Hz, 1H, H$^{7}{}_a$), 4.21 (d, ^3J = 14.3 Hz, 1H, H$^{7}{}_b$), 4.65 (d, ^3J = 14.4 Hz, 1H, H^{16}), 4.85 (d, ^3J = 5.5 Hz, 1H, H^{23}), 4.97 (d, ^3J = 14.2 Hz, 1H, H^{16}), 5.16 (d, ^3J = 5.5 Hz, 1H, H^{22}), 5.57 (d, ^3J = 5.5 Hz, 1H, H^{25}), 5.81 (br s, 1H, H^{20}), 5.87 (d, ^3J = 5.5 Hz, 1H, H^{24}), 7.28 (d, ^3J = 8.6 Hz, 1H, H^{10}), 7.43 (m, 1H, H^2), 7.44 (m, 1H, H^3), 7.45 (m, 1H, H^{11}), 7.77 (d, ^3J = 6.0 Hz, 1H, H^1), 7.80 (s, 1H, H^8), 8.09 (s, 1H, H^{19}), 8.15 (d, ^3J = 6.0 Hz, 1H, H^4), 8.24 (s, 1H, H^{15}), 12.15 (s, 1H, H^{12}), 14.13 (br s, 1H, H^{13}), H^{20} not detected. ^{13}C NMR (100.63 MHz, DMSO-d_6, δ_C, ppm): 16.13 (C^{21}), 19.09 (C^{26}), 21.85 (C^{29}), 22.73 (C^{28}), 23.71 (C^7), 31.26 (C^{27}), 59.18 (C^{16}), 74.08 (C^{22}), 74.54 (C^{25}), 76.36 (C^{24}), 80.55 (C^{23}), 92.32 (C^{23a}), 98.62 (C^{25a}), 110.43 (C^{7a}), 112.61 (C^9), 114.47 (C^{11}), 120.94 (C^8), 124.86 (C^{12b}), 125.42 (C^{10}), 126.12 (C^2), 127.27 (C^1), 127.43 (C^{19}), 128.22 (C^{7b}), 128.50 (C^3), 130.64 (C^4), 131.40 (C^{15b}), 135.23 (C^{12a}), 137.07 (C^{11a}), 139.12 (C^{15a}), 146.22 (C^{19a}), 146.50 (C^{15}), 148.15 (C^{4a}), 154.46 (C^{19b}), 168.28 (C^6). Mp: 200 °C (dec). Single crystals of **2b** $\cdot 1.5C_3H_6O \cdot 0.55H_2O$ suitable for X-ray diffraction study were grown in a solution of **2b** in acetone at 4 °C.

Instrumentation and Methods

Elemental analyses were carried out by the Microanalytical Service at the Institute of Physical Chemistry of the University of Vienna. Thermogravimetric and differential thermal analyses were performed on a Mettler Toledo TGA/SDTA851e instrument. The content of ethanol in the samples was determined by integration of ^{1}H NMR spectra and used for the calculation of the compositions of the prepared compounds. The water content was determined by fitting to elemental analyses and verified by thermogravimetric measurements. IR spectra were recorded on a Perkin-Elmer FT-IR 2000 spectrometer in KBr (4000–400 cm^{-1}). UV–vis spectra were measured on a Perkin-Elmer Lambda 650 UV–vis spectrophotometer, using samples dissolved in methanol or DMSO−water. Electrospray ionization mass spectrometry (ESI-MS) was carried out with a Bruker Esquire 3000 instrument with solutions of the compounds in methanol. Expected and experimental isotope distributions were compared and *m*/*z* values were quoted for the species with highest natural abundance. Cyclic voltammograms were measured in a three-electrode cell using a 0.2-mm-diameter glassy carbon working electrode, a platinum auxiliary electrode, and a Ag|Ag$^+$ reference electrode containing 0.1 M $AgNO_3$. Measurements were performed at room temperature, using an EG&G PARC 273A potentiostat/galvanostat. Deaeration of the solutions was accomplished by passing a stream of argon through the solution for 5 min prior to the measurements and then maintaining a blanket atmosphere of argon over the solutions during the measurements. The potentials were measured in 0.15 M [*n*-Bu_4N][BF_4]−DMF, using Fc/Fc$^+$ ($E_{1/2}$ = +0.72 V vs NHE)[17] as the internal standard, and were quoted relative to Fc/Fc$^+$.

NMR Spectroscopy. ^{1}H, ^{31}P, and ^{13}C and two-dimensional ^{1}H−^{1}H COSY, ^{1}H−^{1}H TOCSY, ^{1}H−^{1}H ROESY, ^{1}H−^{13}C HMQC, ^{1}H−^{13}C HMBC, and ^{1}H−^{15}N COSY NMR spectra were recorded with a Bruker Avance DPX 400 (^{1}H 400.13 MHz, ^{31}P 161.98 MHz, and ^{13}C 100.63 MHz) or a Bruker Avance III 500 (^{1}H 500.10 MHz, ^{31}P 202.44 MHz, ^{13}C 125.75 MHz, and ^{15}N 50.68 MHz) spectrometer in DMSO-d_6 or 90% D_2O and 10% DMSO-d_6 at room temperature, using standard pulse programs. Two-dimensional spectra were measured in a gradient-enhanced mode. ^{1}H and ^{13}C NMR shifts are referenced relative to the solvent signals, and ^{31}P NMR shifts are given relative to those of external H_3PO_4.

Crystallographic Structure Determination. X-ray diffraction measurements were performed on a Bruker X8 APEX II CCD diffractometer. Single crystals were positioned at 40 mm from the detector, and 1020, 1413, 996, and 1924 frames were measured, each for 60, 60, 50, and 30 s over a 1° scan width at 100, 100, 296, and 100 K for $\mathbf{HL^1} \cdot HNO_3$, **1a**, **1b**, and **2b**, correspondingly. The data were processed using *SAINT* software.[18] Crystal data, data collection parameters, and structure refinement details are given in Table 2. The structures were solved by direct methods and refined by full-matrix least-squares techniques. Non-H atoms were refined with anisotropic displacement parameters. H atoms were inserted in calculated positions and refined with a riding model. The following

(18) Pressprich, M. R.; Chambers, M. R. *SAINT+ Integration Engine, Program for Crystal Structure Integration*; Bruker Analytical X-ray Systems: Madison, WI, 2004.

Table 2. Crystal Data and Details of Data Collection for $HL^1 \cdot HNO_3$, 1a, 1b, and 2b

compound	$HL^1 \cdot HNO_3 \cdot CH_3OH$	$1a \cdot C_2H_5OH$	$1b \cdot C_2H_5OH$	$2b \cdot 1.5C_3H_6O \cdot 0.55H_2O$
chemical formula	$C_{24}H_{22}BrN_5O_5$	$C_{35}H_{37}BrCl_2N_4O_2Ru$	$C_{35}H_{37}BrCl_2N_4O_2Os$	$C_{38.5}H_{44.1}BrCl_2N_5O_{4.05}Os$
fw	540.38	797.57	886.70	982.73
space group	$P\bar{1}$	$P2_1$	$P2_1$	$P\bar{1}$
a, Å	9.0821(8)	11.0237(9)	11.0920(10)	13.1551(7)
b, Å	10.9265(9)	11.0373(7)	11.1604(8)	16.7459(9)
c, Å	12.4005(12)	13.7107(11)	13.9373(11)	19.1476(9)
α, deg	71.806(6)			81.092(3)
β, deg	76.420(6)	90.076(6)	90.296(6)	83.527(3)
γ, deg	88.703(6)			72.158(4)
V, Å^3	1134.65(18)	1668.2(2)	1725.3(2)	3957.2(4)
Z	2	2	2	2
d_{calcd}, g cm^{-3}	1.582	1.588	1.707	1.649
μ, cm^{-1}	1.860	1.866	5.046	4.413
T, K	100	100	296	100
R1[a]	0.0320	0.0355	0.0508	0.0375
wR2[b]	0.0803	0.0672	0.0923	0.0928

[a] $R1 = \sum||F_o| - |F_c||/\sum|F_o|$. [b] $wR2 = \{\sum[w(F_o^2 - F_c^2)^2]/\sum[w(F_o^2)^2]\}^{1/2}$.

computer programs were used: structure solution, *SHELXS-97*;[19] refinement, *SHELXL-97*;[20] molecular diagrams, *ORTEP*;[21] computer, Pentium IV; scattering factors.[22]

Cell Lines and Culture Conditions. A549 cells (non-small cell lung carcinoma) and SW480 cells (adenocarcinoma of the colon) were obtained from the American Type Culture Collection and kindly provided by Brigitte Marian, Institute of Cancer Research, Medical University of Vienna, Vienna, Austria. CH1 cells originated from an ascites sample of a patient with a papillary cystadenocarcinoma of the ovary and were kindly provided by Lloyd R. Kelland, CRC Centre for Cancer Therapeutics, Institute of Cancer Research, Sutton, U.K.

Cells were grown in 75 cm^2 culture flasks (Iwaki) as adherent monolayer cultures in a complete culture medium, *i.e.*, Minimal Essential Medium supplemented with 1 mM sodium pyruvate, 4 mM L-glutamine, and 1% non-essential amino acids (100×) (all purchased from Sigma-Aldrich) and 10% heat-inactivated fetal bovine serum (purchased from Invitrogen). Cultures were maintained at 37 °C in a humidified atmosphere containing 5% CO_2.

Antiproliferative Activity in Cancer Cell Lines. Antiproliferative activity was determined by means of a colorimetric microculture assay [MTT assay, MTT = 3-(4,5-dimethyl-2-thiazolyl)-2,5-diphenyl-2*H*-tetrazolium bromide, purchased from Fluka]. For this purpose, A549, CH1, and SW480 cells were harvested from culture flasks by trypsinization and seeded into 96-well microculture plates (Iwaki). The following cell densities were chosen in order to ensure exponential growth throughout drug exposure: 4×10^3 cells well^{-1} for A549, 1.5×10^3 cells well^{-1} for CH1, and 2.5×10^3 cells well^{-1} for SW480. After a 24 h preincubation, cells were exposed to solutions of the test compounds in 200 μL well^{-1} complete culture medium for 96 h. At the end of exposure, drug solutions were replaced by 100 μL well^{-1} RPMI1640 culture medium (supplemented with 10% heat-inactivated fetal bovine serum) plus 20 μL well^{-1} MTT solution in phosphate-buffered saline (5 mg mL^{-1} PBS). After incubation for 4 h, the medium−MTT mixtures were removed, and the formazan crystals formed by the mitochondrial dehydrogenase activity of vital cells were dissolved in 150 μL of DMSO per well. Optical densities at 550 nm were measured with a microplate reader (Tecan Spectra Classic), using a reference wavelength of 690 nm to correct for unspecific absorption. The quantity of vital cells was expressed in terms of *T*/*C* values by comparison to untreated control microcultures, and IC_{50} values were calculated from concentration−effect curves by interpolation. Evaluation is based on means from at least three independent experiments, each comprising six microcultures per concentration level.

Results and Discussion

The kenpaullone derivative 9-bromo-7,12-dihydroindolo[3,2-*d*][1]benzazepin-6-ylhydrazine[8] was used as the starting material for the syntheses of two ligands based on the kenpaullone scaffold (Scheme 1). Upon reaction with 2-hydroxybenzaldehyde and 3-hydroxy-5-(hydroxymethyl)-2-methylpyridinium-4-carbaldehyde chloride, the ligands $\mathbf{HL^1}$ and $\mathbf{HL^2} \cdot$HCl were obtained in 93% and 86% yield, respectively. Their reaction with the organometallic precursors $[M^{II}Cl(\mu\text{-}Cl)(\eta^6\text{-}p\text{-cymene})]_2$ (M = Ru, Os) in ethanol gave rise to complexes of the type $[M^{II}Cl(\eta^6\text{-}p\text{-cymene})HL]Cl$ (**1**, HL = $\mathbf{HL^1}$; **2**, HL = $\mathbf{HL^2}$; **a**, M = Ru; **b**, M = Os). No base was needed for coordination of $\mathbf{HL^2} \cdot$HCl to the ruthenium(II) or osmium(II) arene moiety. However, longer reaction times and slightly elevated temperature (40 °C) were required to compensate for the low solubility of the ligand. The complexes **1a** and **1b** precipitated directly from the reaction mixture, whereas **2a** and **2b** crystallized upon standing at 4 °C because of their higher solubility in ethanol.

Both $\mathbf{HL^1}$ and $\mathbf{HL^2}$ provide an N_2O binding site for metal chelation. The deprotonated ligand $(\mathbf{L^1})^-$ was indeed found to coordinate to the metal in a tridentate meridional manner in the complex $[Ga^{III}(\mathbf{L^1})_2]Cl$.[8] In ruthenium(II) and osmium(II) arene complexes, three facial coordination sites are occupied by the arene ligand. Because the remaining coordination sites have a facial arrangement and the ligands are not flexible enough to span them all, they coordinate in a bidentate fashion (*vide infra*). Only the two N atoms of the binding site act as donors, rendering the aldehyde part with the hydroxy group(s) pendent.

All compounds displayed two resonances in IR spectra in the region from 3183 to 3415 cm^{-1}, attributable to N−H vibrations. The four complexes exhibited absorbance bands at ca. 2970 cm^{-1}, which were ascribed to aliphatic C−H vibrations. Strong vibrations between 1609 and 1626 cm^{-1} assigned to the C=N group were found for $\mathbf{HL^1}$, $\mathbf{HL^2} \cdot$HCl, **1a**, and **1b**.

The UV region of electronic absorption spectra was dominated by two intense bands, one with maxima between 209 and

(19) Sheldrick, G. M. *SHELXS-97: Program for Crystal Structure Solution*; University of Göttingen: Göttingen, Germany, 1997.

(20) Sheldrick, G. M. *SHELXS-97: Program for Crystal Structure Refinement*: University of Göttingen: Göttingen, Germany, 1997.

(21) Johnson, G. K. *Report ORNL-5138*; Oak Ridge National Laboratory: Oak Ridge, TN, 1976.

(22) *International Tables for X-ray Crystallography*; Kluwer Academic Press: Dordrecht, The Netherlands, 1992; Vol. C,Tables 4.2.6.8 and 6.1.1.4.

229 nm and one with maxima between 315 and 319 nm with an intensity of 30–50% of the former for all compounds (Figure S1 in the Supporting Information). Both are likely due to $\pi \rightarrow \pi^*$ transitions within the ligands.[9] For all complexes, one or two further absorption maxima or shoulders were seen in the visible region of the spectra between 360 and 440 nm. Interestingly, similar bands were also observed for **HL²**·HCl. In addition, **2a** and **2b** showed absorption bands at 500 and 520 nm. The yellow (**1a** and **1b**) and red (**2a** and **2b**) colors of the complexes are caused by the mentioned absorbance features in the visible part of the spectrum with $\epsilon = 3600$ (**2a**) or 5400 M^{-1} cm^{-1} (**2b**), which can be attributed to metal-to-ligand charge-transfer $d\pi \rightarrow \pi^*$ transitions because these bands were not observed in the metal-free ligands.

In ESI-MS spectra, **HL²**·HCl displayed peaks at *m/z* 492 and 514 in the positive ion mode, which were attributed to $[\mathbf{HL^2} + H]^+$ and $[\mathbf{HL^2} + Na]^+$, and at *m/z* 490 and 526 in the negative ion mode, resulting from $[\mathbf{HL^2} - H]^-$ and $[\mathbf{HL^2} + Cl]^-$. The corresponding ruthenium complex **2a** showed peaks at *m/z* 726, 762, and 784, attributable to $[RuCl(cymene)\mathbf{HL^2} - HCl]^+$, $[RuCl(cymene)\mathbf{HL^2}]^+$, and $[RuCl(cymene)\mathbf{HL^2} - H + Na]^+$ in the positive ion mode, and at *m/z* 760 and 796 from $[RuCl(cymene)\mathbf{HL^2} - 2H]^-$ and $[RuCl(cymene)\mathbf{HL^2} - H + Cl]^-$ in the negative ion mode. For **1a**, **1b**, and **2b**, additional signals at *m/z* 679, 767, and 848, correspondingly, were also detected and could be assigned to $[MCl(cymene)HL - HCl - 2H]^-$ (**1**; HL = **HL¹**; **2**, HL = **HL²**; **a**, M = Ru; **b**, M = Os).

The paullone ligands **HL¹** and **HL²**·HCl were thermally more stable in the solid state than their organometallic complexes. The paullones decomposed at 240 °C, whereas the complexes showed strongly exothermic degradation, presumably to solid RuO_2 and gaseous OsO_4 at 180 (**1a** and **1b**) and 200 °C (**2a** and **2b**).

The conductometric properties of all complexes with Ph_4PCl as 1:1 electrolyte were determined in DMSO (0.3 μS cm^{-1}) and in methanol (0.8 μS cm^{-1}). The conductivity values of **1a**, **1b**, **2a**, and **2b** were found to lie in the ranges 27.8–31.0 and 73.3–76.6 μS cm^{-1} in DMSO and methanol, respectively, whereas for Ph_4PCl 31.9 and 81.5 μS cm^{-1} were measured in good agreement with the literature data.[23,24] The conductivity values of all complexes are in line with 1:1 electrolytes in solution and suggest that the complex cations remained intact and no solvolysis occurred in these solvents.

In cyclic voltammograms of **HL¹**, two irreversible reduction waves occurred at $E_p = -2.53$ and -2.83 V vs Fc/Fc^+. For **1a** and **1b**, these ligand-centered bands were found at $E_p = -1.67$ and -2.13 V (**1a**) and at $E_p = -1.81$ and -2.28 V (**1b**). Thus, the corresponding potentials were in the order **HL¹** < **1b** < **1a**, with the ruthenium complex showing the most facile reduction. Upon complexation, the separation between the two reduction bands increased from 0.30 to ca. 0.45 V. In the subsequent anodic scan, an oxidation band at $E_p = -0.27$ V (**HL¹**), -0.21 V (**1a**), and -0.03 V (**1b**) was observed in all three cases. Cyclic voltammograms of **HL²**·HCl, **2a**, and **2b** were not conclusive, possibly because of the redox activity of the pyridoxal moiety.

Crystal Structures. Single crystals of **HL¹**·HNO_3 suitable for X-ray diffraction study were obtained during our attempt to synthesize an iron(III) complex, starting from $Fe(NO_3)_3 \cdot 9H_2O$ and **HL¹** in methanol. The result of the X-ray diffraction study of **HL¹**·HNO_3 is shown in Figure 1.

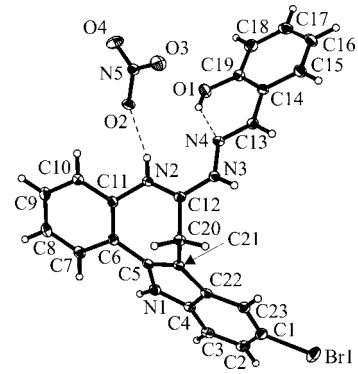

Figure 1. ORTEP view of **HL¹**·HNO_3 with an atom numbering scheme. Thermal ellipsoids are drawn at the 50% probability level. Selected bond distances (Å) and angles (deg): C4−N1 1.373(2), N1−C5 1.378(2), C5−C6 1.454(2), C6−C11 1.414(2), C11−N2 1.4294(19), N2−C12 1.3161(19), C12−N3 1.322(2), C12−C20 1.492(2), C20−C21 1.496(2), C21−C5 1.372(2); C4−N1−C5 108.69(13), C11−N2−C12 127.72(13), N2−C12−N3 121.75(14), N2−C12−C20 120.86(14), N3−C12−C20 117.35(13), C12−C20−C21 106.11(12), $\Theta_{N2-C12-N3-N4}$ −10.2(2), $\Theta_{N3-N4-C13-C14}$ 175.99(14), $\Theta_{N4-C13-C14-C19}$ −4.1(2), $\Theta_{N1-C5-C6-C7}$ 27.0(2); see also Table 1.

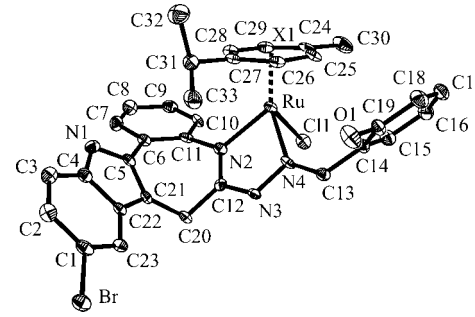

Figure 2. ORTEP view of the cation $[RuCl(p\text{-cymene})\mathbf{HL^1}]^+$ in **1a** with an atom numbering scheme. Thermal ellipsoids are drawn at the 50% probability level. H atoms have been omitted for clarity. Selected bond lengths and angles are summarized in Table 1.

In contrast to previously reported X-ray structures of paullone-based ligands,[9] **HL¹**·HNO_3 crystallized as an amidinium salt with a nitrate as the counterion. The two amidine bonds N2−C12 and C12−N3 possess similar lengths of 1.3161(19) and 1.322(2) Å and are intermediate between a typical single and double bond, *e.g.*, C11−N2 of 1.4294(19) Å and N4−C13 of 1.290(2) Å. All three angles around C12 are close to 120°, indicating its sp^2 hybridization. The presence of the sp^3-hybridized methylene carbon atom C20 leads to the twisted seven-membered azepine ring [characterized by the torsion angle $\Theta_{N1-C5-C6-C7}$ of 27.0(2)°], as observed for all paullones. An intramolecular hydrogen bond O1−H···N4 is evident (O1−H 0.865 Å, H···N4 1.948 Å, O1···N4 2.700 Å, and O1−H···N4 144.47°) because the Schiff base adopts an *E* configuration relative to the N4−C13 double bond. In fact, O1 as the proton donor forms a bifurcated hydrogen bond to both N4 and nitrate oxygen O2 (O1···O2 2.963 Å). In addition, the nitrate oxygen O2 as the proton acceptor is involved in hydrogen bonding with N2 [N2−H 0.804 Å, H···O2 2.059 Å, N2···O2 2.834 Å, and N2−H···O2 161.82°].

In the X-ray structure of **1a** (Figure 2), the two nitrogen atoms N2 and N4 of **HL¹** coordinate to the ruthenium(II) arene moiety. The involvement of N4 in coordination to ruthenium precludes the preservation of the intramolecular O1−H···N4 hydrogen bond found in the metal-free ligand. In contrast to the latter,

(23) Faithful, B. D.; Gillard, R. D.; Tuck, D. G.; Ugo, R. *J. Chem. Soc. A* **1966**, 1185–1188.
(24) Geary, W. J. *Coord. Chem. Rev.* **1971**, *7*, 81–122.

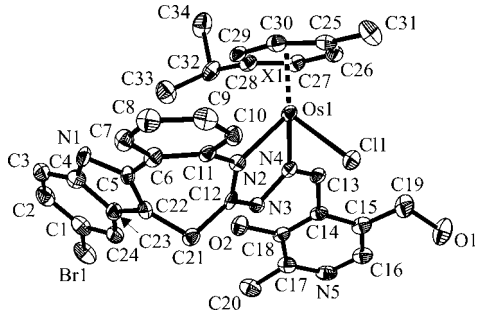

Figure 3. ORTEP view of the first independent cation [OsCl(*p*-cymene)$\mathbf{HL^2}$]$^+$ in **2b** with an atom numbering scheme. Thermal ellipsoids are drawn at the 40% probability level. H atoms have been omitted for clarity. Selected bond lengths and angles are summarized in Table 1.

the bond N2−C12 of 1.291(5) Å is significantly shorter than the bond C12−N3 of 1.353(5) Å, indicating a pronounced double-bond character. The 2-hydroxybenzaldehyde moiety is rotated around the C13−C14 bond so that its hydroxyl group O1H points away from the metal. This orientation is evident from $\Theta_{N4-C13-C14-C19}$, which is −4.1(2)° in metal-free $\mathbf{HL^1}\cdot HNO_3$ and increases to 115.0(5)° in **1a**. The *E* configuration at the N4−C13 double bond is retained upon complexation. Complex **1b** (Figure S4 in the Supporting Information) is isostructural to **1a**, as can be seen from a comparison of crystallographic data (Table 2).

The asymmetric unit of **2b** contains two crystallographically independent complex cations, the first of which is shown in Figure 3. Figure S6 in the Supporting Information shows both independent cations superimposed. Like $\mathbf{HL^1}$, $\mathbf{HL^2}$ is bound to the osmium(II) arene moiety in a bidentate manner via N2 and N4. The main difference between the two independent cations is the orientation of the pyridoxal moiety, as can be seen from the opposite signs of $\Theta_{N4-C13-C14-C18}$ of 37.6(8)° and $\Theta_{N9-C47-C48-C52}$ of −39.3(8)° in the first and second independent cations of **2b**, respectively. This is presumably the result of a $\pi-\pi$ stacking interaction between the pyridoxal moieties of both independent cations (the dihedral angle between the interacting aromatic rings is 12.9°; they are twisted by ca. 60° about the centroid−centroid vector, and the centroid−centroid separation is 3.757 Å, Figure S5 in the Supporting Information). In contrast to **1a** and **1b**, the ligand in **2b** is found in the *Z* configuration, which leads to an approach of O2 to N3. The N5 atom instead of N3 is found to be protonated, like in a number of other compounds containing the pyridoxal moiety.[25,26]

All M−arene centroid, M−N, and M−Cl bond lengths are close to those observed for other ruthenium(II) and osmium(II) arene compounds,[27,28] and bond lengths within the pyridoxal moiety compare well with other pyridoxal Schiff bases.[29,30] However, slight differences are observed between the ruthenium complex **1a** and the osmium complexes **1b** and **2b**. While the bond lengths M−N2 and M−N4 are equal within 3σ[31] for **1a** and **1b**, they differ by 7.1σ for **2b**. A different situation is observed for C12−N2 and C12−N3 at the coordinated amidine unit, which differ by 8.8σ in **1a** and are equal for **1b** and **2b**. The azepine ring is twisted, with the methylene carbon atom pointing away from the cymene ligand in all complexes possibly for steric reasons.

Scheme 2. Amidine Tautomerization and Amidinium Ion[a]

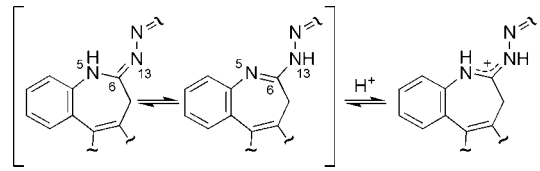

[a] Atom labeling is as in Chart 2.

^{1}H NMR Spectra. ^{1}H NMR spectra of $\mathbf{HL^1}\cdot HNO_3$, which was found to be protonated at the amidine moiety in its X-ray structure (*vide supra*), showed one set of signals. In contrast, $\mathbf{HL^1}$ displayed two signal sets with different intensities, each corresponding to a tautomer with either an exocyclic $C^6{=}N^{13}$ or an endocyclic $C^6{=}N^5$ double bond.[8] This indicates that protonation at the amidine group leads to an amidinium ion, where the resulting positive charge is delocalized over both amidine C−N bonds, impeding tautomerization (Scheme 2).

In ^{1}H NMR spectra of $\mathbf{HL^2}\cdot HCl$ recorded immediately after dissolution, two tautomers are observed with relative abundances of 59% and 41%, based on peak integrals. Their relative intensities did not change over time. This implies that $\mathbf{HL^2}\cdot HCl$ remained protonated at the N atom of the pyridoxal moiety in the solid state and in DMSO. The tautomer with an exocyclic amidine double bond (more abundant species) showed H^5 at 10.70, whereas the other tautomer displayed H^{13} at 14.05 ppm. Similarly, H^{12} resonances were observed at 12.07 (exocyclic) and 12.01 ppm (endocyclic). Because of fast inversion of the seven-membered azepine ring, methylene protons H^7 were displayed as a singlet for both tautomers at 3.84 (exocyclic) and 4.00 ppm (endocyclic).

In all complexes, a single set of signals with diastereotopic H^7 protons was found which indicates that neither azepine ring inversion nor *E*/*Z* isomerization at the $N^{14}{=}C^{15}$ double bond took place in the solution. When **1a** and **1b** were compared with **2a** and **2b**, it became apparent that all cymene protons except H^{26} experienced a significant upfield shift in the complexes of $\mathbf{HL^1}$. The resonances were shifted to higher field in **1a** compared to **2a**: H^{22} by 0.29 ppm, H^{23} by 0.38 ppm, H^{24} by 0.88 ppm, H^{25} by 1.15 ppm, H^{27} by 0.24 ppm, H^{28} by 0.19 ppm, and H^{29} by 0.13 ppm (Figure 4). That a β-phenyl effect[32] accounts for the observed upfield shifts is evident from the crystal structures of **1a** and **1b**. The pendent phenyl group is oriented so that the cymene protons lie within its anisotropy cone (Figures 2, S4 and S7 in the Supporting Information). In particular, H^{24} and H^{25}, which are on the side pointing toward the pendent moiety, experience the most pronounced shift. This interaction is not possible in **2a** and **2b** because the paullone ligands adopt the *Z* configuration relative to the $N^{14}{=}C^{15}$ bond in these complexes. In all complexes, H^{13} was found as a broad resonance in the range 14.13–15.23 ppm. An H^{20} signal was

(25) Murphy, T. B.; Rose, N. J.; Schomaker, V.; Aruffo, A. *Inorg. Chim. Acta* **1985**, *108*, 183–194.
(26) Domiano, P.; Musatti, A.; Nardelli, M.; Pelizzi, C.; Predieri, G. *Inorg. Chim. Acta* **1980**, *38*, 9–14.
(27) Ciancaleoni, G.; Bellachioma, G.; Cardaci, G.; Ricci, G.; Ruzziconi, R.; Zuccaccia, D.; Macchioni, A. *J. Organomet. Chem.* **2006**, *691*, 165–173.
(28) Peacock, A. F. A.; Habtemariam, A.; Fernández, R.; Walland, V.; Fabbiani, F. P. A.; Parsons, S.; Aird, R. E.; Jodrell, D. I.; Sadler, P. J. *J. Am. Chem. Soc.* **2006**, *128*, 1739–1748.
(29) Souron, J.-P.; Quarton, M. *Acta Crystallogr.* **1995**, *C51*, 2179–2182.
(30) Sharif, S.; Powell, D. R.; Schagen, D.; Steiner, T.; Toney, M. D.; Fogle, E.; Limach, H.-H. *Acta Crystallogr.* **2006**, *B62*, 480–487.
(31) Clegg, W.; Blake, A. J.; Gould, R. O.; Main, P. *Crystal Structure Analysis*; International Union of Crystallography, Oxford University Press: Oxford, U.K., 2001.
(32) Brunner, H. *Angew. Chem., Int. Ed.* **1983**, *22*, 879–907.

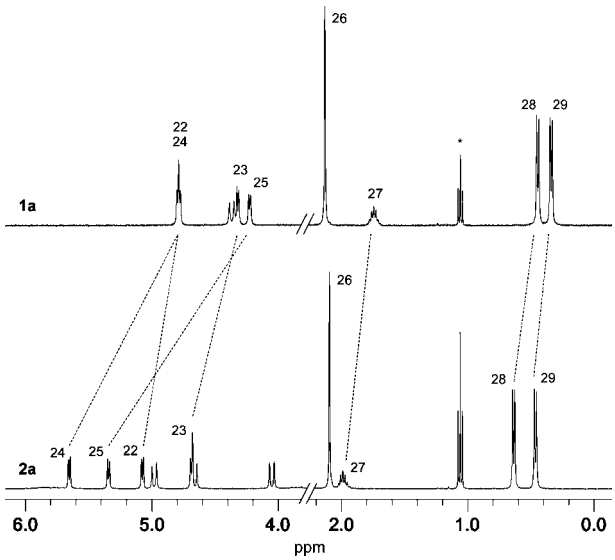

Figure 4. ^{1}H NMR spectra of **1a** (upper trace) and **2a** (lower trace), showing a β-phenyl effect for **1a**. An ethanol signal is marked with an asterisk; unlabeled signals at 4.48 ppm in **1a** and at 4.06, 4.66, and 4.99 ppm in **2a** with larger coupling constants result from methylene groups.

Chart 2. NMR Atom Numbering Scheme and Cymene Orientation

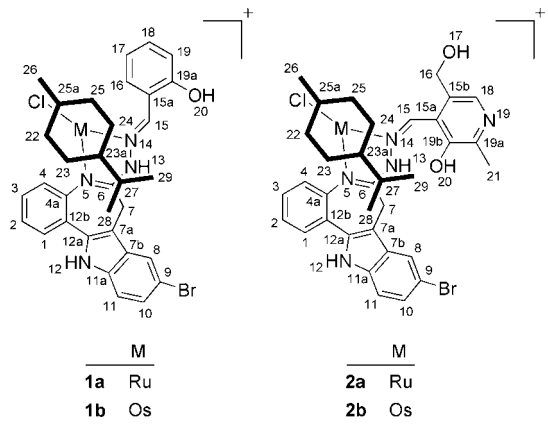

detected in **1a** and **1b** at 10.79 and 10.76 ppm, respectively, while this resonance was not observed in spectra of **2a** and **2b**.

Two-Dimensional NMR Spectra and Assignments. All ^{1}H and ^{13}C NMR resonances of the novel complexes could be assigned by using ^{1}H−^{1}H COSY, ^{1}H−^{1}H TOCSY, ^{1}H−^{1}H ROESY, ^{1}H−^{13}C HMQC, ^{1}H−^{13}C HMBC, and ^{1}H−^{15}N COSY NMR experiments (Chart 2 and Tables S1 and S2 in the Supporting Information). ^{1}H−^{1}H ROESY NMR spectra of **1a** and **1b** were found to be consistent with the structures of these complexes in the solid state. The close similarity of NMR spectra (^{1}H, ^{13}C, and ^{1}H−^{1}H ROESY) of **2a** and **2b** indicated that both complexes possess the same structure in the solid state and in solution. The ^{1}H−^{15}N COSY NMR spectrum of **1a** allowed the differentiation of NH from OH proton resonances.

In solution, the same cymene ligand orientation as that in the solid state was observed for **1a** and **1b**, which was indicated by strong NOE contacts H^{16}/H^{25} and H^4/H^{22} and weak H^{16}/H^{24} and H^4/H^{23} (**1a**: Figure S8 in the Supporting Information). For **2a**, strong NOE crosspeaks H^{15}/H^{24} and H^{15}/H^{25}, medium H^4/H^{22}, and weak H^4/H^{23} (Figure S9 in the Supporting Information) are in agreement with the similar cymene ligand orientations observed in the two independent molecules in the crystal structure of **2b** (Figure S6 in the Supporting Information). Presumably, the approach of the cymene ligand toward the paullone scaffold caused by coordination at the azepine N atom no longer allows its rotation around the M−cymene centroid vector.

The adopted *Z* configuration of the Schiff base in **2a** was confirmed by NOE crosspeaks between H^{15} and cymene protons (Figure S9 in the Supporting Information). In contrast, NOE contacts between H^{16} and cymene protons were detected for **1a** (Figure S8 in the Supporting Information) and **1b**, in agreement with an *E* configuration of the Schiff base in the complexes. A ^{1}H−^{1}H ROESY NMR spectrum enabled the distinction of diastereotopic azepine high-field $H^7{}_a$ and low-field $H^7{}_b$ methylene protons. The NOE crosspeak $H^7{}_b/H^8$ is clearly seen, while $H^7{}_a/H^8$ is absent. As a consequence, $H^7{}_b$ was assigned to the methylene proton pointing toward H^8 and $H^7{}_a$ to the proton above the azepine ring.

Studies of Hydrolysis. The time-dependent behavior of all complexes in DMSO solutions diluted with water was studied by ^{1}H NMR in 90% D_2O and 10% DMSO-d_6 at 37 °C and by UV–vis in 95% H_2O and 5% DMSO at room temperature over 72 h (Figure S2 in the Supporting Information). A comparison of NMR spectra measured directly after dissolution with those obtained after treatment of the samples with 2 equiv of $AgNO_3$ provided evidence of fast hydrolysis for all complexes in D_2O/DMSO-d_6 solvent mixtures. Two sets of signals attributed to chlorido and aqua complexes accounted for approximately 30% and 70% in all solutions.

In NMR spectra recorded 0.5 h after dissolution, the chlorido complexes could no longer be detected. Instead, a signal set[33] with a pattern typical of free cymene appeared. In particular, the isopropylmethyl groups displayed as a doublet and the aromatic protons as a doublet of doublets, and all resonances were shifted by only 0.2–0.3 ppm to higher field, compared to the δ reported for metal-free cymene in $CDCl_3$.[34] In all cases studied, the amount of free cymene remained constant after 24 h. Arene loss in an aqueous solution has been reported to compete with hydrolysis for various $[RuCl(p\text{-cymene})(azpy)]^+$ (azpy = azopyridine) complexes.[35] Because of the comparably low achievable concentrations and the high rate of hydrolysis, the disappearance of the chlorido complexes could not be followed by kinetic NMR experiments.

It should be noted that a solid precipitated slowly from the solutions of **1a** and **1b** used for NMR measurements, whereas no precipitation was observed in the more dilute solutions used for the determination of antiproliferative properties and for UV–vis measurements. For **2a** and **2b**, two further cymene species A and B in addition to the chlorido and aqua complexes were detected immediately after dissolution. After 0.5 h for **2a**, the four mentioned cymene species and two cymene-free paullone species C and D were observed (31% free cymene, 23% species B, 19% species C, 15% species A, 8% aqua complex, and 4% species D). The spectrum of **2b** displayed five or six cymene species with overlapping signal sets, including species A. Because species A had shifts and signal

(33) ^{1}H NMR chemical shifts of free cymene: 1.12 (d, J = 6.9 Hz, 6H, isopropylmethyl groups), 2.21 (s, 3H, methyl group), 2.80 (sept, J = 6.9 Hz, 1H, isopropyl proton), and 7.13 and 7.17 ppm (both d, J = 7.8 Hz, 2H, aromatic protons).

(34) Herberhold, M.; Yan, H.; Milius, W. *J. Organomet. Chem.* **2000**, *598*, 142–149.

(35) Dougan, S. J.; Melchart, M.; Habtemariam, A.; Parsons, S.; Sadler, P. J. *Inorg. Chem.* **2006**, *45*, 10882–10894.

patterns[36] comparable to those of free cymene, it was likely a small cymene-derived molecule. After the highest concentration was reached after 24 h in the case of **2a** and already after 0.5 h in the case of **2b**, transient species A disappeared, as shown by subsequently measured spectra. Also, species B, containing a [Ru(*p*-cymene)(paullone ligand)] fragment, was detected only in the spectrum recorded after 0.5 h for **2a**.

After 72 h at 37 °C, spectra of **2a** indicated the presence of metal-free cymene (ca. 50%) and the two cymene-free paullone species C and D (which accounted for ca. 40% and 10%, respectively). Both paullone species were coordinated to Ru, as evidenced by their diastereotopic H^7 resonances. Presumably, these were the species responsible for the appearance of an additional absorption band at 450 nm (Figure S2 in the Supporting Information) in 95% H_2O and 5% DMSO. ESI-MS spectra of this NMR sample diluted with methanol showed a peak at *m/z* 992 in the negative mode. The isotopic pattern agrees with the presence of Ru and Br and the absence of Cl in this species.

Similarly, spectra of **2b** after 72 h showed metal-free cymene (ca. 55%), two paullone species (ca. 32% and 13%, respectively), and a small amount (<5%) of an unidentified species. In contrast to **2a**, diastereotopic H^7 resonances as well as corresponding cymene signals were detected for the two paullone species, indicating that cymene and the paullone ligand remained Os-bound. As for **2a**, ESI-MS spectra of this NMR sample diluted with methanol did not show peaks assignable to the assumed hydrolysis products.

Reactivity toward 5′-GMP. The reactions of all complexes with 5′-GMP in an equimolar ratio in 90% D_2O and 10% DMSO-d_6 at 37 °C were studied by ^1H and ^{31}P NMR spectroscopy over 72 h. Although a small amount of precipitate formed in the NMR tube of **1a**, an additional ^{31}P NMR signal at 0.49 ppm was detected already after 0.5 h and reached its maximum of 27% of total 5′-GMP (0.07 ppm) after 24 h. The 5′-GMP H^8 NMR resonance was shifted by 0.44 ppm from 8.27 to 8.71 ppm, which is close to 8.73 ppm, as observed for the N^7-(5′-GMP) adduct of $[Ru(biphenyl)(en)]^{2+}$.[37] The observed small ^{31}P NMR shift is also in line with the assignment to an N^7 adduct. After 72 h, another weak ^{31}P NMR signal at −0.26 ppm was detected (7% of the total 5′-GMP). The corresponding osmium complex **1b** did not react with 5′-GMP under the conditions applied for **1a**.

The reaction of **2a** with 5′-GMP was not as fast as that of **1a**; no additional ^{31}P NMR resonance was observed after 0.5 h. After 24 h, however, a second and even more intense signal than that of unreacted 5′-GMP was found at 0.71 ppm, which did not show a further increase in its intensity after 48 h. After 72 h, four new species and unreacted 5′-GMP with ^{31}P NMR resonances at 0.71, 0.67, 0.08 (5′-GMP), −0.07, and −0.88 ppm and relative abundances of 47%, 10%, 31%, 5%, and 8% were detected. The most abundant species displayed a 5′-GMP H^8 resonance shifted by 0.77 ppm from 8.26 to 9.03 ppm. The species with ^{31}P NMR resonances at lower field compared to free 5′-GMP are assignable to N^7 adducts, whereas resonances at higher field possibly result from cGMP species or species where 5′-GMP is bound to O^{17} or O^{20} of the complexes via its P atom. Like **1b**, the osmium complex **2b** did not react with 5′-GMP under the conditions applied for **2a**.

(36) ^1H NMR chemical shifts of species A: 0.77 (d, $J = 6.9$ Hz, 6H, isopropyl groups), 1.77 (s, 3H, methyl group), and 6.55 and 6.59 (both d, $J = 6.9$ Hz, 2H, aromatic protons), isopropyl proton probably superimposed.

(37) Chen, H.; Parkinson, J. A.; Morris, R. E.; Sadler, P. J. *J. Am. Chem. Soc.* **2003**, *125*, 173–186.

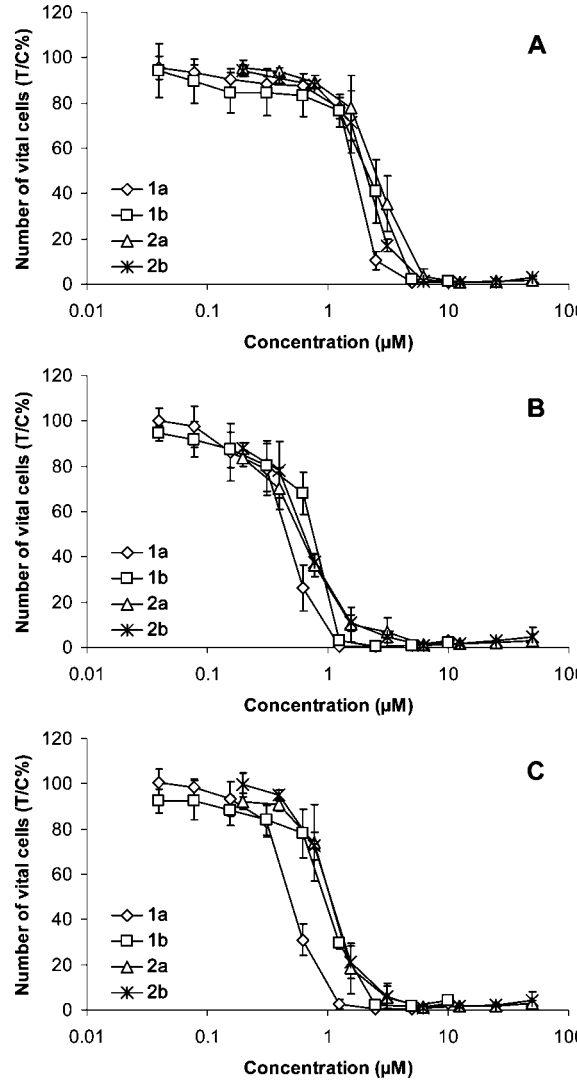

Figure 5. Concentration−effect curves of ruthenium (**1a** and **2a**) and osmium (**1b** and **2b**) arene complexes in A549 (A), CH1 (B), and SW480 (C) cells, obtained by the MTT assay.

Table 3. Antiproliferative Activity of Ruthenium Complexes (1a and 2a) and Osmium Complexes (1b and 2b) in Three Human Cancer Cell Lines

	IC_{50} (μM)[a]		
compound	A549	CH1	SW480
1a	1.7 ± 0.1	0.53 ± 0.18	0.59 ± 0.19
1b	2.2 ± 0.5	0.75 ± 0.07	1.2 ± 0.4
2a	2.5 ± 0.6	0.58 ± 0.08	1.0 ± 0.2
2b	2.0 ± 0.2	0.63 ± 0.09	1.0 ± 0.1

[a] 50% inhibitory concentrations in A549, CH1, and SW480 cells after exposure for 96 h in the MTT assay. Values are means ± standard deviations, obtained from at least three independent experiments.

Antiproliferative Activity in Cancer Cell Lines. Antiproliferative activity of the ruthenium (**1a** and **2a**) and osmium (**1b** and **2b**) complexes described herein was tested in three human cancer cell lines (A549, CH1, and SW480) by means of the colorimetric MTT assay with 96 h exposure. Concentration−effect curves are depicted in Figure 5, and IC_{50} values are listed in Table 3. A comparison with the metal-free paullone derivatives $\mathbf{HL^1}$ and $\mathbf{HL^2}\cdot$HCl was not possible because of their insufficient aqueous solubility.

In general, the investigated complexes show respectable antiproliferative activity in submicromolar to very low micro-

molar concentrations in all three cell lines. The rank order of sensitivities of the cell lines is identical for all four complexes: CH1 (ovary) ≥ SW480 (colon) > A549 (lung). Estimated IC_{50} values are in the ranges of 0.53−2.5 and 0.63−2.2 μM for ruthenium (**1a** and **2a**) and osmium complexes (**1b** and **2b**), respectively. Hence, the osmium complexes **1b** and **2b** range among the most potent osmium compounds reported so far.[38,39]

No clear-cut structure–activity relationships can be deduced from these data. Only the ruthenium arene complex **1a** seems to be slightly more active than the analogue **2a** and the corresponding osmium analogues (**1b** and **2b**), but differences are not very pronounced. Thus, these effects are largely independent of the central metal atom (ruthenium or osmium), suggesting that direct interactions between the central metal and target molecules are unlikely. Likewise, neither the configuration nor the moiety bound at the azomethine double bond has a conclusive influence on the antiproliferative activity.

The finding that ruthenium and osmium analogues do not differ in their biological activity to a meaningful extent has important implications for the mechanism of action. Hydrolysis and interaction with 5′-GMP indicate differences in the solution behavior of the ruthenium and osmium compounds. As a third-row transition-metal ion, Os^{II} might also be expected to be relatively inert compared to the second-row ion Ru^{II}.[40] So, different antiproliferative activity profiles would be expected if coordinative DNA binding was the main mode of action for both the ruthenium(II) and osmium(II) complexes. Therefore, either noncovalent DNA binding such as, *e.g.*, intercalation, as previously suggested for paullone coordination compounds[9] or protein interactions such as those reported for metal-free paullones (*vide supra*) are more likely to account for the antiproliferative effects.

Conclusion

The possibility of binding paullones to ruthenium(II) and osmium(II) arene scaffolds has been demonstrated via the synthesis of organometallic compounds of the general formula $[M^{II}Cl(\eta^6\text{-}p\text{-cymene})HL]Cl$ (**1**, HL = **HL^1**; **2**, HL = **HL^2**; **a**, M = Ru; **b**, M = Os). Potentially tridentate paullone ligands coordinate to Ru^{II} and Os^{II} in a bidentate fashion via two N atoms, as shown by X-ray crystallography. This binding resulted in enhanced aqueous solubility, which made the paullones bioavailable and allowed testing for antiproliferative activity.

Rapid hydrolysis was found in water−DMSO mixtures, and further concurrent transformations were observed for **2a** and **2b**. Metal−paullone bonds remained intact in aqueous solution. Suppression of hydrolysis is of major concern for any attempt to develop compounds of this kind for clinical application. Being evident in this case, the enormous problems for the development of metal-based drugs in general, posed by the requirements pertaining to the quantification, identification, and safety qualification of drug degradation products exceeding certain low thresholds must not be underestimated. Probably much more so than in the case of purely organic agents, these requirements are an insurmountable obstacle for many classes of metal complexes.

Because comparably high antiproliferative activity in cancer cell lines was observed for all complexes despite marked differences in 5′-GMP binding, we expect the complexes to exert their effects either by binding to crucial proteins or by noncovalent DNA interactions such as, *e.g.*, intercalation.

In addition, a notable crystallographic contribution has been made in this work. The compounds **1a**, **1b**, and **2b** expand the relatively small number of metal-based paullone derivatives[8,9] characterized by X-ray diffraction.

Acknowledgment. We thank A. Roller for the collection of X-ray data sets.

Supporting Information Available: CIF files for **HL^1**·HNO_3, **1a**, **1b**, and **2b**; UV–vis spectra of all compounds; time dependence of the absorption at 450 nm of **2a**; ORTEP view of the cation $[OsCl(p\text{-cymene})\mathbf{HL^1}]^+$ in **1b**; superimposed X-ray structures of both independent cations of **2b**; relative orientation of the pyridoxal moieties in both independent cations of **2b**; superimposed X-ray structures of the cations of **2b** and **1b**; sections of the $^1H-^1H$ ROESY NMR spectra of **1a** and **2a**; assigned ^1H and ^{13}C NMR shifts of all compounds. This material is available free of charge via the Internet at http://pubs.acs.org.

OM700813C

(38) Peacock, A. F. A.; Parsons, S.; Sadler, P. J. *J. Am. Chem. Soc.* **2007**, *129*, 3348–3357.

(39) Peacock, A. F. A.; Habtemariam, A.; Moggach, S. A.; Prescimone, A.; Parsons, S.; Sadler, P. J. *Inorg. Chem.* **2007**, *46*, 4049–4059.

(40) Shriver, D. F.; Atkins, P. W. *Inorganic Chemistry*, 3rd ed.; Oxford University Press: Oxford, U.K., 1999.